Journal of Materials Chemistry A

Accepted Manuscript

This article can be cited before page numbers have been issued, to do this please use: E. de la Llave, P. K. Nayak, E. Levi, T. R. Penki, S. Bublil, P. Hartmann, F. F. Chesneau, M. Greenstein, L. Nazar and D. Aurbach, *J. Mater. Chem. A*, 2017, DOI: 10.1039/C6TA10577G.

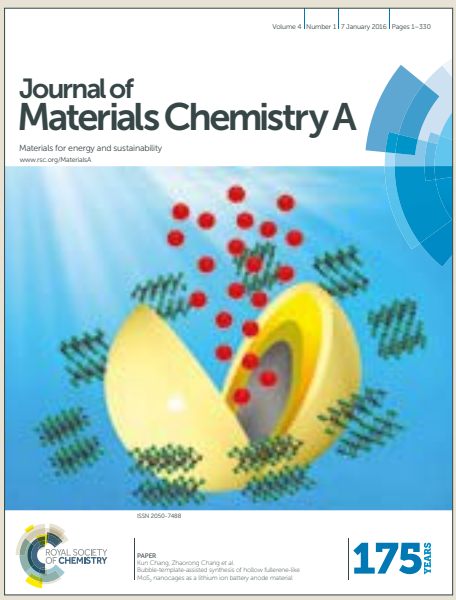

ROYAL SOCIETY OF CHEMISTRY

rsc.li/materials-a

View Article Online
DOI: 10.1039/C6TA10577G

Electrochemical performance of $Na_{0.6}[Li_{0.2}Ni_{0.2}Mn_{0.6}]O_2$ cathodes with high-working average voltage for Na-ion batteries

Ezequiel de la Llave[a†], Prasant Kumar Nayak[a†], Elena Levi[a], Penki Tirupathi Rao[a], Shaul Bublil, Pascal Hartmann[c], Frederick- Francois Chesneau[c] Miri Greenstein[a], Linda F. Nazar[b], Doron Aurbach[a]*

[a]Chemistry Department, Bar-Ilan University, Ramat-Gan 5290002, Israel

[b]Department of Chemistry and the Waterloo Institute of Nanotechnology, University of Waterloo, Waterloo, ON N2L 3G1, Canada

[c]BASF SE, Ludwigshafen 67056, Germany

[†] equal contributions
*Corresponding author
Doron.Aurbach@biu.ac.il (Doron Aurbach)

View Article Online
DOI: 10.1039/C6TA10577G

Abstract

$Na_{0.6}[Li_{0.2}Ni_{0.2}Mn_{0.6}]O_2$ is synthesized by a self-combustion reaction (SCR) and studied for the first time as a cathode material for Na-ion batteries. The $Na_{0.6}[Li_{0.2}\ Ni_{0.2}Mn_{0.6}]O_2$ cathode presents remarkable high rate capability and prolonged stability under galvanostatic cycling. A detailed analysis of X-ray diffraction (XRD) patterns at various states of cycling reveals that the excellent structural stability is due to a primarily solid-solution sodiation/desodiation mechanism of the material during cycling. Moreover, a meaningful comparison with $Na_{0.6}MnO_2$ and $Na_{0.6}[Li_{0.2}Mn_{0.8}]O_2$ reveals that the $Na_{0.6}[Li_{0.2}\ Ni_{0.2}Mn_{0.6}]O_2$ cathode achieves a very high working-average voltage that outperforms most of the lithium-doped manganese-oxide cathodes published to date.

Key words: Na-ion batteries, cathode material, high average working voltage

View Article Online
DOI: 10.1039/C6TA10577G

1. Introduction

Due to their high energy density and long life cycle, Li-ion batteries have become a major power source, with applications in portable electronic devices.[1-4] Despite their high energy density, however, the anticipated rise in cost of Li (driven by the increasing market intrusion of Li-ion batteries for vehicular transport) has prompted the search for other intercalation materials. Sodium-based batteries are considered as the most promising alternative. Although rechargeable sodium-ion batteries (NIB) are inferior to Li-ion technology in terms of energy density, they appear to be one of the most promising technologies for stationary large-scale energy storage devices.[5-6] Because of the high abundance and low cost of sodium compared to lithium, there is increasing interest in these systems.[7-9]

Layered oxide compounds are particularly promising as the positive electrodes of NIB due to their high specific capacities.[10-15] While these materials were introduced during the early1980s,[16-19] it was recently discovered that Na-ion-based cathodes can exhibit specific capacities close to 200 mAh g^{-1}, making them an excellent choice for energy-storage devices.[20-23] Although promising, layered transition metal oxides exhibit capacity fading due to the structural instability resulting from the intercalation/de-intercalation of large Na^+ ions[24-26] and migration of transition metal cations into the interlayer space.[26-27] Recently, it was found that structural doping of lithium in manganese oxides enhances the structural stabilization of the cathodes upon cycling.[26-32] Nonetheless, these oxide cathodes exhibit a low average discharge voltage compared to their Li-based cathode analogs, limiting their practical energy density.

In this paper, we report for the first time the electrochemical performance of $Na_{0.6}[Li_{0.2}Ni_{0.2}Mn_{0.6}]O_2$ synthesized by a self-combustion reaction (SCR) as a cathode for NIB.

View Article Online
DOI: 10.1039/C6TA10577G

The material analyzed here outperforms any other lithium-doped manganese oxide published to date, in terms of average working voltage and rate capability, as well as high structural stability.

2. Experimental section

Analytical-grade chemicals, namely, $Mn(NO_3)_2$ (Fluka), $Ni(NO_3)_2$, $NaNO_3$, $LiNO_3$ (Aldrich), sucrose, poly(vinylidene fluoride) (PVDF) and 1-methyl-2-pyrrolidinone (NMP) (Aldrich) were used as received. Double distilled (DD) water was used to dissolve the metal nitrates and sucrose.

2.1. Synthesis and structural characterization

In a typical SCR synthesis,[33] 1.454 g of $Ni(NO_3)_2$, 3.765 g of $Mn(NO_3)_2$, 0.362 g of $LiNO_3$ and 1.340 g of $NaNO_3$ were dissolved in 80 ml of DD water. About 5 wt% of Li and Na nitrates were used in excess to compensate for the Li and Na loss upon annealing at a high temperature. Sucrose was then added to the continuously stirred solution. Next, the water was evaporated by heating at about 100 °C for a few hours to obtain a syrupy mass, which on further heating at 350 °C resulted in the self-ignition of the reactants and, subsequently, an amorphous compound. This product was ground to a fine powder, annealed at 500 °C for 3 h and cooled down to room temperature. The obtained powder was then ground and finally annealed at 900 °C for 15 h, to obtain the desired oxide material.

Elemental analysis of the synthesized material was carried out using the inductive coupled plasma technique (ICP-AES, spectrometer Ultima-2 from JobinYvon Horiba). X-ray diffraction (XRD) studies were performed with a Bruker Inc. (Germany) AXS D8 ADVANCE diffractometer (reflection θ-θ geometry, Cu Kα radiation, receiving slit 0.2 mm, high-resolution

View Article Online
DOI: 10.1039/C6TA10577G

energy-dispersive detector). The morphology of the products was investigated by a Magellan XHR 400L FE-SEM-FEI scanning electron microscope.

Electrode preparation: The cathode electrodes were fabricated by mixing 80 wt% of the cathode material, 10 wt% of carbon black and 10 wt% of PVDF binder. A planetary centrifugal vacuum mixer was used to shake the vials at 2000 rpm for 10 min under vacuum. The obtained slurry was cast onto aluminum foil, followed by coating with a doctor blade. The electrodes were then dried overnight at 80 °C under vacuum. The resulting foil was cut into discs 14 mm in diameter, which were weighed and dried at 110 °C overnight in vacuum, in order to remove the moisture adsorbed during the preparation process. A typical loading of the active mass was 3-4 mg cm^{-2}. The electrochemical performance was examined using 2325 coin-type cells assembled in an argon-filled dry glovebox (MBraun). Na metal foil was used for the counter and reference electrodes.

Battery testing was carried out using multichannel battery testers (Arbin Inc.). The galvanostatic charge-discharge cycling experiments were carried out at 12 mA g^{-1} (C/15 rate) over the potential range of 2.0-4.6 V vs. Na. Electrochemical impedance spectroscopy (EIS) experiments were measured using a VMP Bio-Logic Potentiostat with a 1287/1260 FRA system from Solartron. For all the experiments, the selected electrolyte solution was 0.5 M $NaPF_6$ in PC.

3. Results and discussion

The XRD pattern of the $Na_{0.6}[Li_{0.2}Ni_{0.2}Mn_{0.6}]O_2$ powder is shown in **Figure 1**. The crystal structure can be assigned to a hexagonal P2 structure within the $P6_3/mmc$ space group, which is isostructural with P2-$Na_{2/3}CoO_2$, as previously reported by Paulsen and Dahn.[10] All the observed

View Article Online
DOI: 10.1039/C6TA10577G

Bragg diffraction peaks exhibit a long coherence length (beyond that detectable by XRD broadening), which shows the high degree of crystallinity of the synthesized sample. The XRD pattern resembles other previously published lithiated manganese oxides with a hexagonal P2 structure.[26-32] The weak peak near 19° (marked by an asterisk in **Figure 1**) can be assigned to the presence of a secondary Li_2MnO_3 phase, as previously reported for a similar material.[31] The morphology of the powder is presented in the scanning-electron-microscopy (SEM) image in the inset. The image shows well-crystallized particles of dimensions in the range of 300-500 nm, in good agreement with the morphology of the $Na_{0.6}MnO_2$ and $Na_{0.6}[Li_{0.20}Mn_{0.80}]O_2$ cathodes recently synthesized by our group using SCR.[26] From ICP elemental analysis, the powder-chemical composition is found to be $Na_{0.60}[Li_{0.22}Ni_{0.20}Mn_{0.58}]O_2$, which is very close to the target composition.

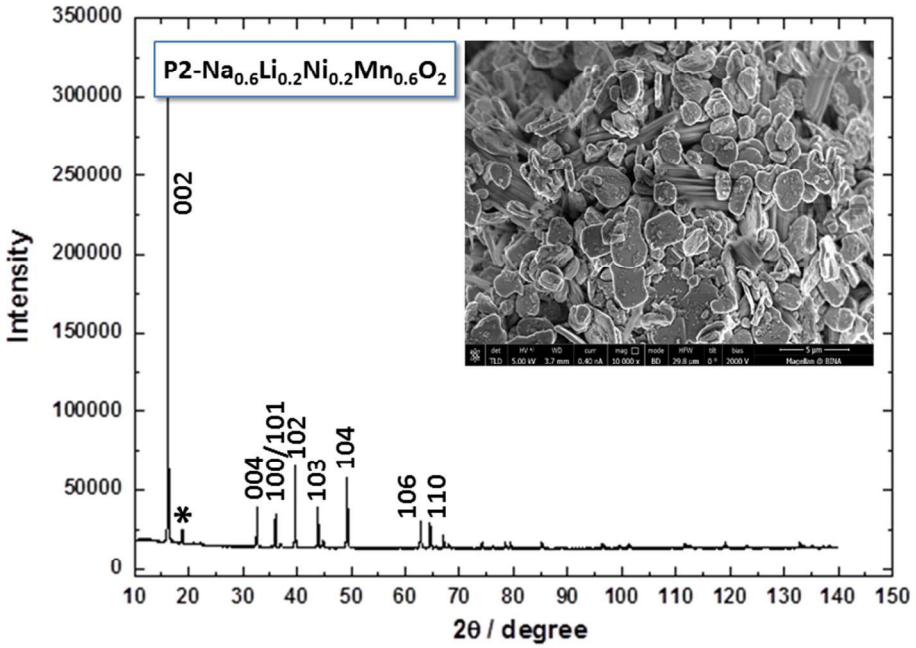

Figure 1. XRD pattern of $Na_{0.6}Li_{0.2}$ $Ni_{0.2}Mn_{0.6}O_2$ powder. Inset: SEM image of the sample.

View Article Online
DOI: 10.1039/C6TA10577G

The electrochemical behavior of $Na_{0.6}[Li_{0.2}Ni_{0.2}Mn_{0.6}]O_2$ as cathode material for sodium-ion batteries is shown in **Figure 2**, which is illustrative of typical galvanostatic charge-discharge curves (panel a) and differential dQ/dV vs. V profiles (panel b) for our cathode material at different cycling stages. The cells were charged to 4.6 V (vs Na) and then discharged to 2.0 V (vs Na) at a constant rate (12 mA/g ~ C/15 rate) in standard coin-type cells. The first-cycle voltage profile gradually slopes upward, followed by a plateau at about 4.4 V vs. Na. This same feature can be clearly seen as a sharp peak at about 4.4 V in the differential capacity plot in **Figure 2b**, along with a smaller peak at about 4.0 V which is discussed below. Together with the voltage profile, the differential capacity plot reveals that the 4.4 V process only takes place during the first cycle. This process can be ascribed to the partial activation of the Li_2MnO_3 secondary phase observed in the XRD pattern of **Figure 1**, which is well known to occur in lithium and manganese-rich cathode materials for LIB.[34-44]

From the voltage profile it can be clearly seen that the initial specific capacity increases from about 130 mAh/g to roughly 150 mAh g^{-1} during the first cycles. After the 50^{th} cycle, the capacity slightly decreases, reaching a constant value at about 120 mAh/g for more than 100 cycles. Several broad peaks correspond to the intercalation/deintercalation of Na^+ ions to/from the crystal lattice in the differential capacity plot. Recent XAS experiments on similar materials proves that Ni is the only electrochemically active species involved on the charge compensation during charge/discharge process, whereas Mn remains inactive.[28-29] The incremental increase in capacity during the first cycle observed in our material is probably due to a partial activation of the manganese on the Li_2MnO_3 secondary phase, unleashed during charge at high voltage.

View Article Online
DOI: 10.1039/C6TA10577G

After the first step, no significant changes are observed in the shape of the voltage profiles or the differential capacity plot, which is evidence of the structural stability of the cathode material. More interestingly, the smooth voltage profile and the broader peaks on the differential capacity plots suggest that the principal mechanism involved in the sodiation/desodiation process is based on a solid-solution process instead of two-phase transitions. In recent work,[25-26] we showed that, during cycling, the sodium manganese oxides undergo a detrimental multi-phase transition which induces structural instability. Also, we proved that this structural instability can be overcome by lithium-structural doping, which has a direct effect on the insertion/deinsertion mechanism. In addition, we demonstrated that the presence of lithium dopant effectively reduces the extent of the detrimental Jahn-Teller distortions in the material, due to the increase in the average manganese oxidation state.[26] Similar considerations are valid for the $Na_{0.6}[Li_{0.2}Ni_{0.2}Mn_{0.6}]O_2$ cathode analyzed in this paper.

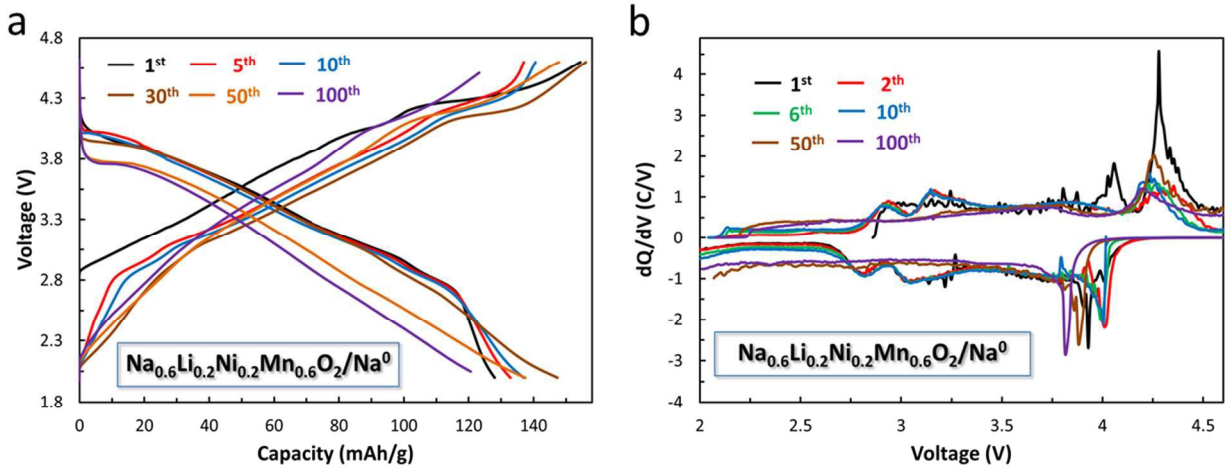

Figure 2. Electrochemical performance of $Na_{0.6}[Li_{0.2}Ni_{0.2}Mn_{0.6}]O_2$ cathodes. Panel a: galvanostatic charge/discharge curves. Panel b: dQ/dV vs. V (voltage profile derivatives). The experiments were performed at 30 °C at a rate of C/15 (~12 mA/g) in 0.5 M $NaPF_6$ PC electrolyte solution.

View Article Online
DOI: 10.1039/C6TA10577G

In order to further explore the sodiation/desodiation mechanism, *ex-situ* XRD measurements at charge (4.6 V) and discharge (2.0 V) states were examined (**Figure 3**). After cycling, the cells were opened inside a dry glovebox under a pure argon atmosphere, thoroughly washed with dry PC solvent several times and left to dry inside the glovebox. The electrodes were transferred to the X-ray diffractometer in hermetically sealed holders in order to avoid any reaction with the atmosphere prior to the XRD pattern acquisition. **Figure 3** also shows the XRD patterns of both the pristine cathode and the cathode after prolonged cycling.

The XRD pattern on charge state conserve the main features of the pristine P2-phase, revealing that no phase transition take place during charge. The determination of the unit cell parameters by profile matching, showed an increase in the interlayered distance of about 1.9 % in charged state, with respect to the pristine sample (11.042 Å vs 11.253 Å). This is probably due to the enhancement of the repulsion between the MO_2 sheets, which increases as de-sodiation takes place.

At a fully-discharged state, the XRD pattern is virtually identical to that of the pristine sample, confirming the full reversibility of the charge/discharge process described above. However, the XRD pattern evolution reveals that the small peak located around 19^0, which was identified as a secondary Li_2MnO_3 phase, significantly decreased in intensity during cycling. This finding gives further confirmation to the activation process proposed above. **Figure 3** also presents the XRD pattern after 100 galvanostatic cycles at a fully discharged state. In comparison to the pristine cathode, the main features of the XRD pattern after the prolonged cycle are conserved, confirming the excellent structural stability of the cathode material. Also, no evidence of the presence of the Li_2MnO_3 phase was found. A slight shifts and peak broadening are

View Article Online
DOI: 10.1039/C6TA10577G

observed, probably due to the accumulation of stacking faults after prolonged sodiation/desodiation cycling, as previously reported for similar materials.[24]

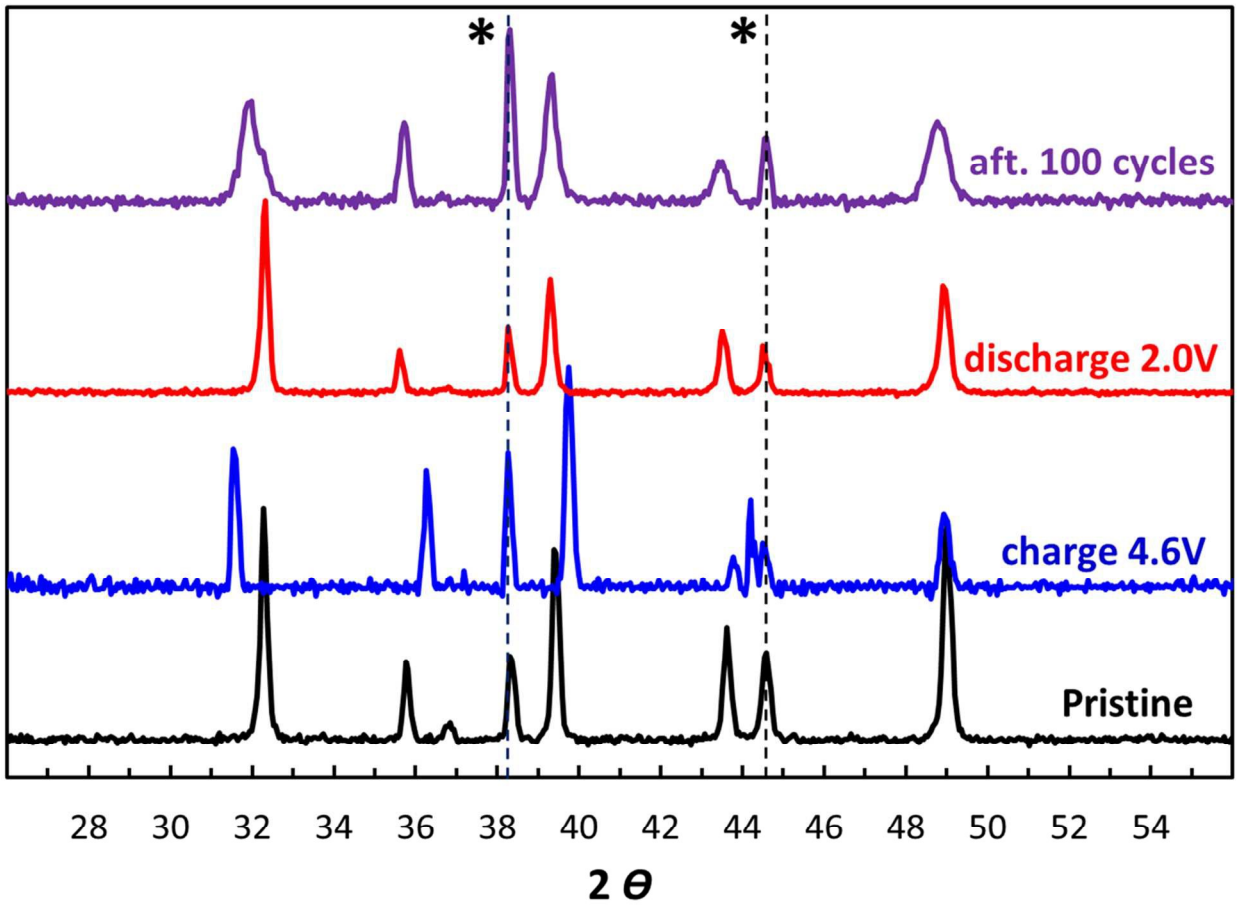

Figure 3. *Ex-situ* XRD patterns. Charge (4.6 V) and discharge (2.0 V) state during the second galvanostatic cycle were investigated. The pattern of the pristine cathode (black curve) and the cathode after 100 galvanostatic cycles in discharge state (purple curve) are plotted for comparison. Black asterisks denote the signals related to the aluminium current collector.

To provide a comprehensive picture of the structural stability of our cathode material, the electrochemical behavior of the cathodes, under prolonged galvanostatic cycles, is presented. **Figure 4** shows both the discharge capacity and the coulombic efficiency, of the $Na_{0.6}[Li_{0.2}Ni_{0.2}Mn_{0.6}]O_2$ cathode in conventional coin-type half cells with 0.5 M $NaPF_6$ PC solutions at 30 °C. The cell was charged up to 4.6 V and then discharged to 2.0 V (vs Na), and cycled at a rate of C/15.

View Article Online
DOI: 10.1039/C6TA10577G

The first cycle delivery possesses an initial discharge capacity of 126 mAh/g, with a coulombic efficiency of 81%. This low coulombic efficiency is linked to the process occurring during the activation process during first cycle described above. After the first cycle, the total capacity of the cathode steadily increased up to 147 mAh/g at the 30th cycle. This capacity remained stable until the 50th cycle, slightly decreasing after that, reaching a constant value of about 120 mAh/g for more than 100 cycles, with a remarkable coulombic efficiency close to 100% during cycling. Recently, we showed that the specific capacity of $Na_{0.6}MnO_2$ decreases rapidly upon cycling. However, the doping of Li in the transition metal layer results in the stabilization of the structure which, in turn, results in improved electrochemical performance, as reported for $Na_{0.6}[Li_{0.2}Mn_{0.8}]O_2$.[26]

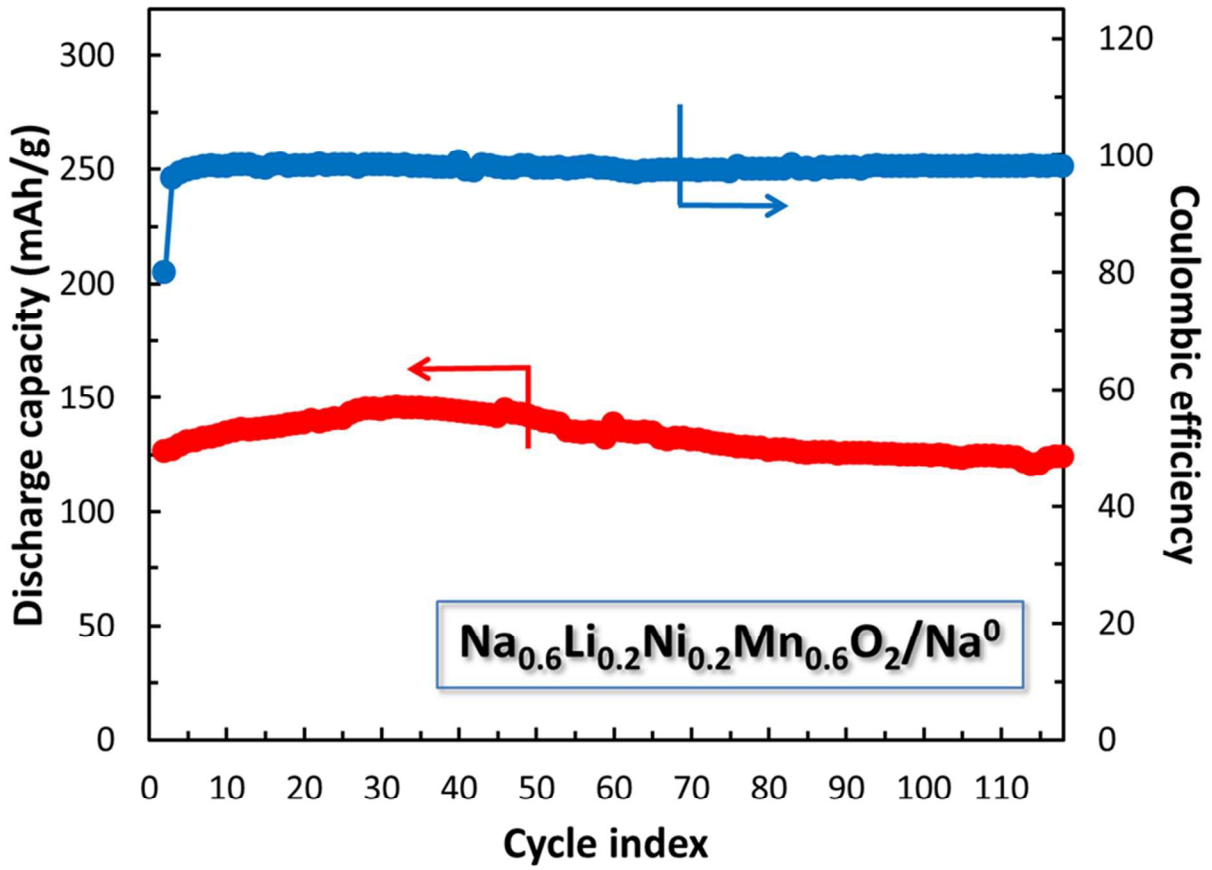

Figure 4. Electrochemical performance of $Na_{0.6}Li_{0.2}Ni_{0.2}Mn_{0.6}O_2$ cathodes. Discharge capacity

View Article Online
DOI: 10.1039/C6TA10577G

(red curve) and coulombic efficiency (blue curve) over the galvanostatic cycle between 4.6 and 2.0 V (vs Na) at 12 mA/g (~ C/15 rate) in standard coin-type cells. The experiments were performed at 30 °C in 0.5 M $NaPF_6$ PC electrolyte solution.

Further confirmation of the cathode stability by lithium doping was obtained by EIS. EIS is an important electro-analytical technique for evaluating the surface phenomenon related to the diffusion of Na^+ ions through a surface film, as well as bulk charge transfer resistance and solid-state diffusion kinetics of Na^+ into the active mass.[45] The impedance was measured at several equilibrium potentials during charging after the completion of 30 charge-discharge cycles at a rate of C/15 (**Figure 5a**). The Nyquist plots present a semicircle at high to medium frequency ranges, representing the parallel combination of resistance (due to surface film and charge-transfer at electrode/electrolyte interface) and double-layer capacitance (C_{dl}). A low frequency linear spike appears, due to the diffusion of Na^+ ions into the active mass. It can be seen that the diameter of the semicircle gradually decreases upon charging to higher potentials, indicating that the resistance due to surface and bulk decreases upon charging. Moreover, a sharp change on the slope of the spectra in the Warburg region (low frequencies) is observed when the cell is charged above 4.0V (**Figure 5a**). This drastic change of the Na^+-ion diffusion in the bulk of the material is a direct consequence of the expantion of the P2-phase observed at low sodium content described above (**Figure 3**).

It is essential to compare the impedance upon prolonged cycling with that obtained after only a few cycles, which can give useful information about the stability of the material. The impedance was measured at a discharged state (about 2.2 V) as well as a charged state (4.6 V) after completing 10, 50 and 100 cycles (**Figures 5b** and **5c**). It can be clearly seen that the diameter of the semicircle initially decreases, indicating the decrease in resistance due to lowered

View Article Online
DOI: 10.1039/C6TA10577G

surface resistance as well as bulk resistance upon cycling from 10 to 50 cycles. The decrease in the resistance is in direct relationship to the increase in capacity observed during the first cycles. Upon further cycling, the Nyquist plots remain almost unchanged, revealing the excellent stability of our cathode material, allowing prolonged cycling in a wide potential range. Thus, the impedance correlates well with the cycling stability of $Na_{0.6}[Li_{0.2}Ni_{0.2}Mn_{0.6}]O_2$, as discussed above.

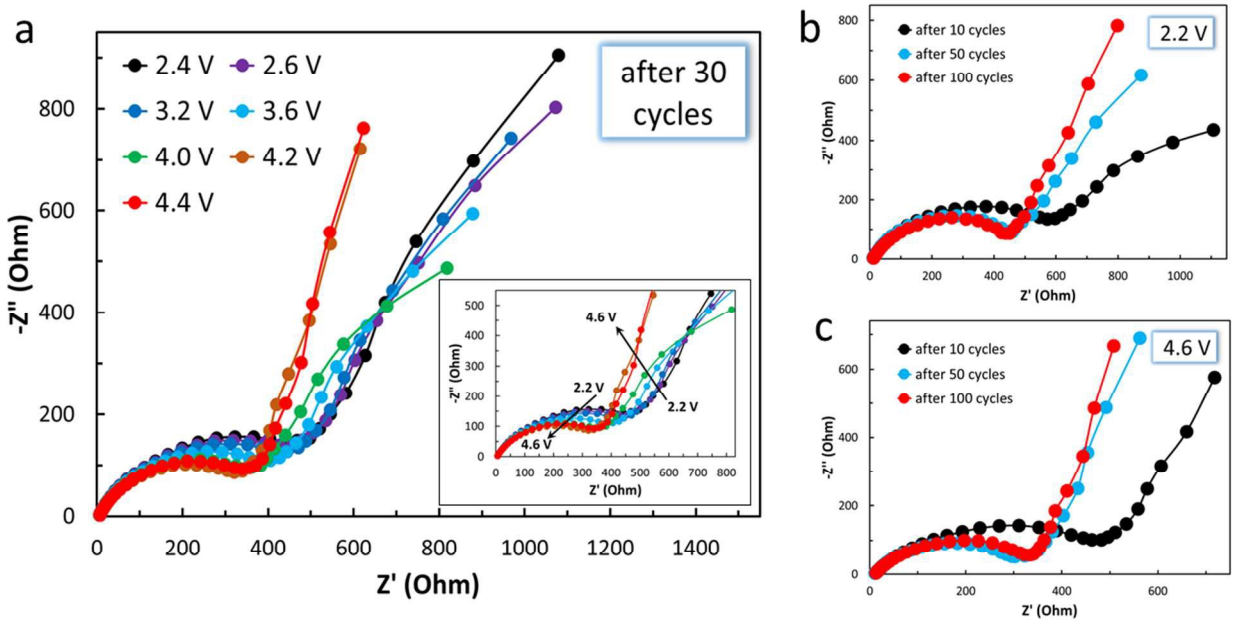

Figure 5. EIS of $Na_{0.6}Li_{0.2}Ni_{0.2}Mn_{0.6}O_2$ cathodes in sodium half-cells. Nyquist plots at different potentials after 30 galvanostatic cycles (panel a), and at different cycling steps in discharge (panel b) and charge (panel c) states. The experiments were performed at 30 °C in 0.5 M $NaPF_6$ PC electrolyte solution.

The cathode material furthermore presents very good rate capability (**Figure 6**). The cell was first run over 20 cycles at a low rate (C/20) until it reached a stable reversible capacity of 145 mAh/g. Increasing the rates to C/10 and C/5 shows a reduction of 8% (134 mAhg) and 21% (120 mAh/g) in capacity, respectively. Interestingly, exceptional capacity values were found at high rates, i.e. 112, 105, 98 and 92 mAh/g for C/2, C, 1.5C and 2C, respectively. Upon returning

View Article Online
DOI: 10.1039/C6TA10577G

to a rate of C/20, the initial high specific capacity was recovered, indicating that the high-rate cycling does not deteriorate the electrochemical stability of the $Na_{0.6}[Li_{0.2}Ni_{0.2}Mn_{0.6}]O_2$ material. This remarkable rate-dependent behavior is accompanied by a highly stable average potential. At the lower rate tested (C/20), the average charge and discharge voltage were 3.55 and 3.13 V, respectively, while at the higher rate (2C), the average charge and discharge voltage changed by only about 7% (3.85 V and 2.90 V, respectively) (**Figure 6**, inset).

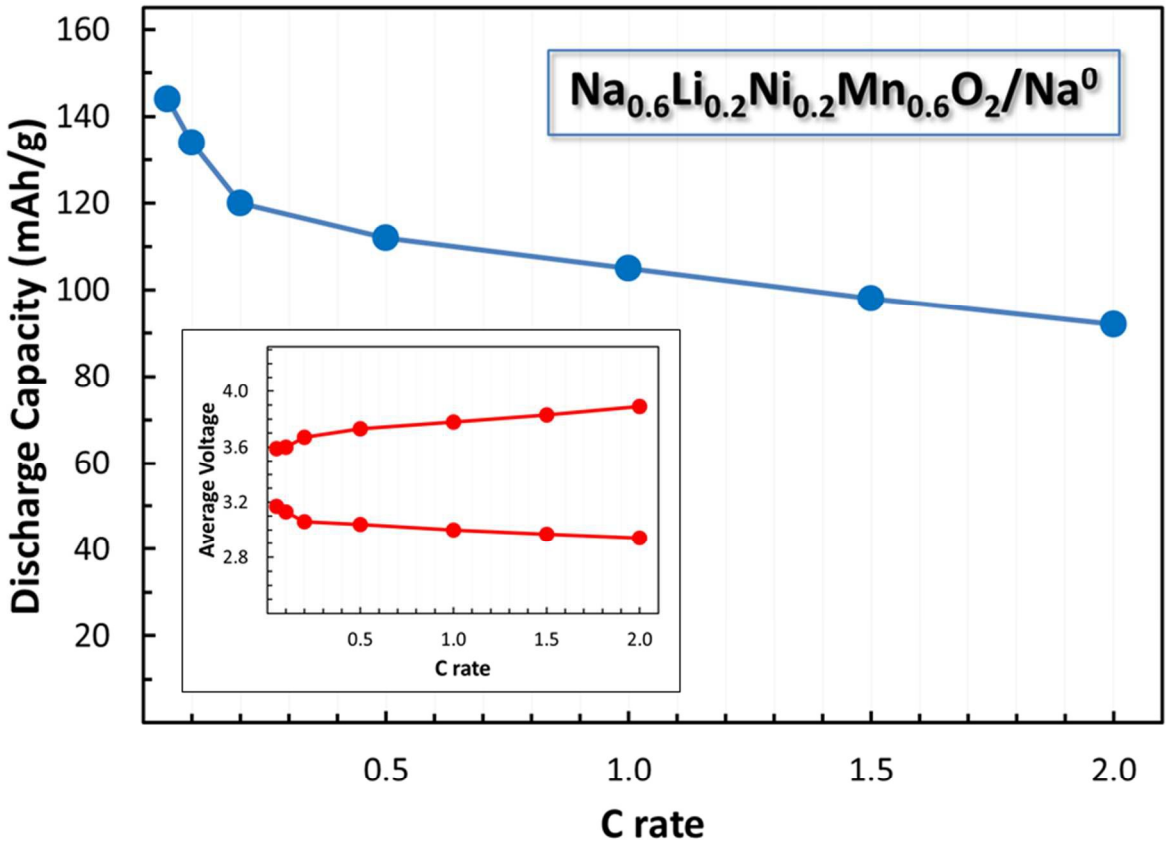

Figure 6. Discharge capacity and average voltage (inset) of $Na_{0.6}Li_{0.2}Ni_{0.2}Mn_{0.6}O_2$ cathodes in sodium half-cells at different current rates (C/10 ~ 16 mA/g). The experiments were performed at 30 °C in 0.5 M $NaPF_6$ PC electrolyte solution.

The excellent rate capabilities of the material appear to arise from a combination of factors; one being the quasi-solid solution behavior over much of the electrochemical profile, and

View Article Online
DOI: 10.1039/C6TA10577G

the other being the partial substitution of manganese for nickel in the lattice. The latter conclusion is well supported by the fact that the increase in Ni content results in an increase in the rate capability and discharge potential in both LIB[40] [40] and NIB,[27] although this is still not well understood. In order to provide a clear picture of the effect of lithium and nickel substitution on the average working voltage of the manganese oxide cathodes in NIB, we compared the voltage profile of the $Na_{0.6}MnO_2$ and $Na_{0.6}Li_{0.2}Mn_{0.8}O_2$ cathodes to our $Na_{0.6}Li_{0.2}Ni_{0.2}Mn_{0.6}O_2$ material (**Figure 7**). The cells were charged to 4.6 V (vs Na) and then discharged to 2.0 V (vs Na) at the same rate (12 mA/g ~ C/15 rate), in standard coin-type cells. The voltage profiles of the cathodes are plotted after they reach a stable reversible capacity, namely, after 40 cycles for the $Na_{0.6}Li_{0.2}Mn_{0.8}O_2$ and $Na_{0.6}Li_{0.2}Ni_{0.2}Mn_{0.6}O_2$ cathodes, and after five cycles for $Na_{0.6}MnO_2$. For more details on the electrochemical behavior of the $Na_{0.6}MnO_2$ and $Na_{0.6}Li_{0.2}Mn_{0.8}O_2$ cathodes, we refer the reader to our recent paper.[26] [26].

Even though the nickel manganese lithium-doped material has the lowest capacity of the tested cathodes – $Na_{0.6}Li_{0.2}Mn_{0.8}O_2$ ~190 mAh/g, $Na_{0.6}MnO_2$ ~160 mAh/g and $Na_{0.6}Li_{0.2}Ni_{0.2}Mn_{0.6}O_2$ ~150 mAh/g – the presence of nickel offers a significant improvement in the cell average voltage. The non-doped material ($Na_{0.6}MnO_2$) shows an average voltage of ~2.7 V, which rises to 2.9 V on lithium substitution ($Na_{0.6}Li_{0.2}Mn_{0.8}O_2$). Moreover, the manganese and nickel cathode ($Na_{0.6}Li_{0.2}Ni_{0.2}Mn_{0.6}O_2$) presents an average voltage of ~3.4 V, outperforming the non-doped $Na_{0.6}MnO_2$ by 0.7 V. This average voltage is among the highest reported in the literature for sodium oxides as cathodes in sodium-ion batteries.[24] In a recent paper Hasa et. al.[27] compared the electrochemical behavior of different P-type layered Na_xMO_2 with M = Ni, Fe, Mn. In the same line with our findings, they showed that the nickel content

View Article Online
DOI: 10.1039/C6TA10577G

remarkably influences the average working potential of the batteries and that the Ni-rich cathodes present the higher structural stability during cycling.

As discussed previously, the increase in the average voltage on the lithiated cathodes may be due not only to the presence of nickel, but also to the contribution of oxide ions in the redox reactions.[26] This hypothesis is being explored in a parallel study and is beyond the scope of this work.

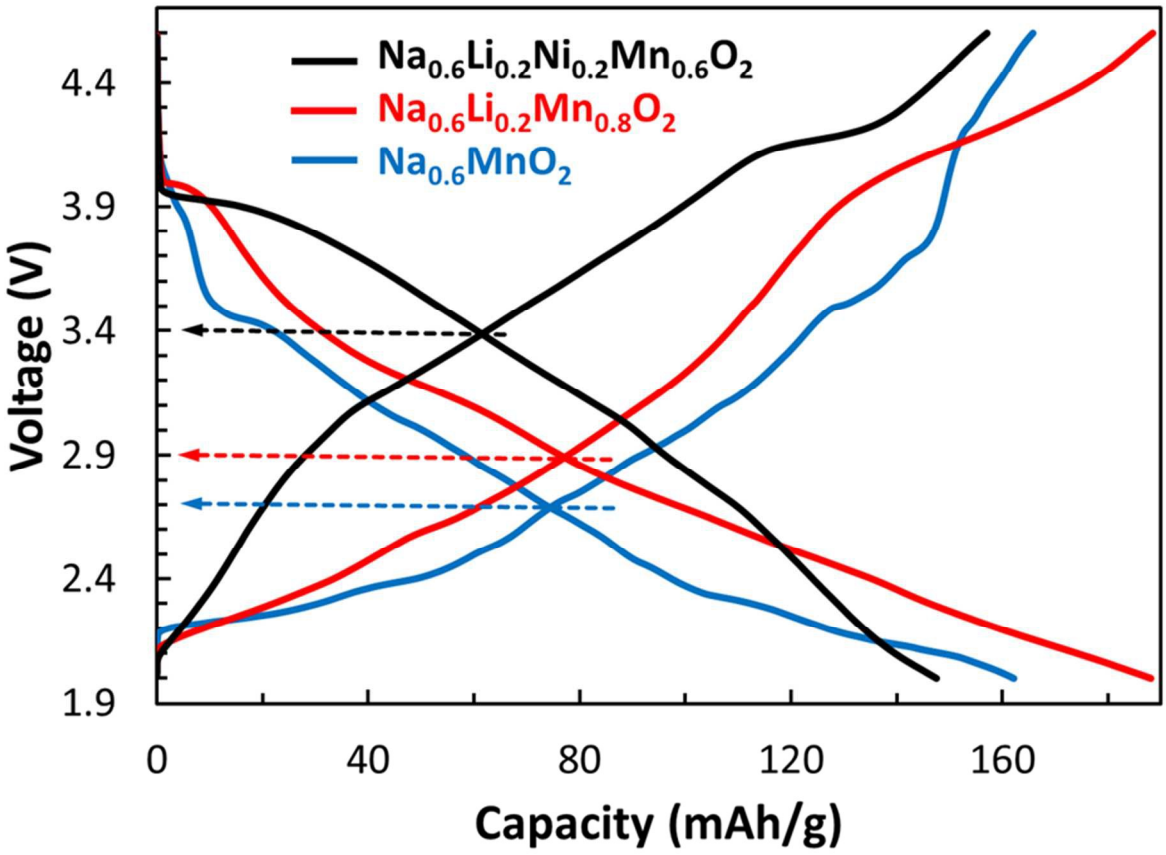

Figure 7. Voltage profile for $Na_{0.6}MnO_2$ (blue), $Na_{0.6}Li_{0.2}Mn_{0.8}O_2$ (red) and $Na_{0.6}Li_{0.2}Ni_{0.2}Mn_{0.6}O_2$ (black). The arrows indicate the average voltage in each case.

View Article Online
DOI: 10.1039/C6TA10577G

4. Conclusions

We demonstrate the advantages of the use of lithiated sodium nickel-manganese oxides as cathodes for sodium-ion batteries. $Na_{0.6}[Li_{0.2}Mn_{0.6}Ni_{0.2}]O_2$ was synthesized by SCR, and the electrochemical behavior as a cathode on sodium-ion cells has been reported for the first time. The incorporation of lithium dopant improves the structural stability, allowing the retention of stable capacity for more than 100 cycles. Through an *ex-situ* XRD analysis at different charge/discharge states, we demonstrated that the principal intercalation mechanism that the material undergoes during galvanostatic cycling is predominately solid-solution. The presence of the lithium dopant appears to be an effective method to partially suppress both the extent of the destructive cooperative Jahn-Teller distortions and detrimental phase transitions. Moreover, the $Na_{0.6}[Li_{0.2}Ni_{0.2}Mn_{0.6}]O_2$ cathode presents an exceptionally high working average voltage, outperforming most of the lithium-doped manganese-oxide cathodes published to date. This work serves as a proof of concept that the careful selection of the proper dopants improves the properties of the manganese oxide intercalation materials, opening the door to the development of cost-effective practical sodium-ion batteries.

Acknowledgement

L.F.N and D.A gratefully acknowledge funding from BASF SE for ongoing support through the BASF Research Network in Electrochemistry and Batteries. Partial support for this work was obtained from the Israel Science Foundation (ISF) as part of the INREP project, and from the Israel Ministry of Science and Technology as part of the Israel-India cooperation program.

View Article Online
DOI: 10.1039/C6TA10577G

References

[1] B. Kennedy, D. Patterson, S. Camilleri, *J. Power Sources* 2000, **90***,* 156-162.

[2] M. Armand, J.-M. Tarascon, *Nature* 2008, **451**, 652-657.

[3] T. Kojima, T. Ishizu, T. Horiba, M. Yoshikawa, *J. Power Sources* 2009, **189**, 859-863.

[4] V. Etacheri, R. Marom, R. Elazari, G. Salitra, D. Aurbach, *Energy Environ. Sci.* 2011, **4**, 3243-3262.

[5] S. W. Kim, D. H. Seo, X. M. Ma, G. Ceder, *Adv. Energy Mater.* 2012, **2**, 710-721.

[6] H. Pan, Y.-S. Hu, L. Chen, *Energy Environ. Sci.* 2013, **6**, 2338-2360.

[7] M. D. Slater, D. Kim, E. Lee, C. S. Johnson, *Adv. Funct. Mater.* 2013, **23**, 947-958.

[8] N. Yabuuchi, K. Kubota, M. Dahbi, S. Komaba, *Chem. Rev.* 2014, **114**, 11636-11682.

[9] D. Kundu, E. Talaie, V. Duffort, L. F. Nazar, *Angew. Chem. Int. Ed*. 2015, **54**, 3431-3448.

[10] J. M. Paulsen, J. R. Dahn, *Solid State Ion.* 1999, **126**, 3-24.

[11] V. Palomares, P. Serras, I. Villaluenga, K. B. Hueso, J. Carretero-Gonzalez, T. Rojo, *Energy Environ. Sci.* 2012, **5**, 5884-5901.

[12] V. Palomares, M. Casas-Cabanas, E. Castillo-Martínez, M. Han, T. Rojo, *Energy Environ. Sci.* 2013, **6**, 2312-2337.

[13] Z. Jian, H. Yu, H. Zhou, *Electrochem. Commun.* 2013, **34**, 215-218.

[14] K. Kubota, N. Yabuuchi, H. Yoshida, M. Dahbi, S. Komaba, *MRS Bull.* 2014, **39**, 416-422.

[15] M. H. Han, E. Gonzalo, G. Singha, T. Rojo, *Energy Environ. Sci.* 2015, **8**, 81-102.

[16] C. Delmas, J.-J. Braconnier, C. Fouassier, P. Hagenmuller, *Solid State Ionics* 1981, **3**, 165-169.

View Article Online
DOI: 10.1039/C6TA10577G

[17] J.-J. Braconnier, C. Delmas, P. Hagenmuller, *Mater. Res. Bull.* 1982, **17**, 993-1000.

[18] S. Miyazaki, S. Kikkawa, M. Koizumi, *Synth. Met.* 1983, **6**, 211-271.

[19] A. Maazaz, C. Delmas, P. Hagenmuller, *J. Inclusion Phenom.* 1983, **1**, 45-51.

[20] R. Kataoka, T. Mukai, A. Yoshizawa, T. Sakai, *J. Electrochem. Soc*. 2013, **160**, A933-A939.

[21] N. Yabuuchi, R. Hara, M. Kajiyama, K. Kubota, T. Ishigaki, A. Hoshikawa, S. Komaba, *Adv. Energy Mater.* 2014, **4**, 1301453.

[22] N. V. Nghia, P.-W. Ou, I.-M. Hung, *Electrochim. Acta* 2015, **161**, 63–71.

[23] J. Xu, D. H. Lee, R. J. Clèment, X. Yu, M. Leskes, A.J. Pell, G. Pintacuda, X.-Q. Yang, C. P. Grey, Y.-S. Meng, *Chem. Mater.* 2014, **26**, 1260-1269.

[24] R. J. Clement, P. G. Bruce, C. P. Grey, *J. Electrochem. Soc*. 2015, **162**, A2589-A2604.

[25] E. de la Llave, V. Borgel, K. J. Park, J. Y. Hwang, Y.-K. Sun, P. Hartmann, F. F. Chesneau, D. Aurbach, *ACS Appl. Mater. Interfaces* 2016, **8**, 1867–1875.

[26] E. de la Llave, E. Talaie, E. Levi, P. K. Nayak, M. Dixit, P. T. Rao, P. Hartmann, F. F. Chesneau, D. T. Major, M. Greenstein, D. Aurbach, L. F. Nazar, *Chem. Mater.* 2016, DOI: 10.1021/acs.chemmater.6b04078

[27] I. Hasa, D. Buchholz, S. Passerini, J. Hassoun, *ACS Appl. Mater. Interfaces* 2015, **7**, 5206-5212.

View Article Online
DOI: 10.1039/C6TA10577G

[28] D. Kim, S.-H. Kang, M. Slater, S. Rood, J. T. Vaughey, N. Karan, M. Balasubramanian, C. S. Johnson, *Adv. Energy Mater.* 2011, **1**, 333-336.

[29] N. K. Karan, M. Slater, F. Dogan, D. Kim, C. S. Johnson, M. Balasubramanian, *J. Electrochem. Soc*. 2014, **6**, A1107-A1115.

[30] E. Lee, J. Lu, Y. Ren, X. Luo, X. Zhang, J. Wen, D. Miller, A. DeWahl, S. Hackney, B. Key, D. Kim, M. D. Slater, C. S. Johnson, *Adv. Energy Mater.* 2014, **4**, 1400458.

[31] N. V. Nghia, P.-W. Ou, I.-M. Hung, *Ceram. Int.* 2015, **41**, 10199-10207.

[32] H. Liu, J. Xu, C. Ma, Y. S. Meng, *Chem. Commun.* 2015, **51**, 4693-4696.

[33] P. K. Nayak, J. Grinblat, M. Levi, B. Markovsky, D. Aurbach, *J. Electrochem. Soc.* 2014, **161**, A1534-A1547.

[34] A. R. Armstrong, M. Holzapfel, P. Novak, C. S. Johnson, S. H. Kang, M. M. Thackeray, P. G. Bruce, *J. Am. Chem. Soc.* 2006, **128**, 8694-8698

[35] D. Y. W. Yu, K. Yanagida, Y. Kato, H. Nakamura, *J. Electrochem. Soc*. 2009, **156**, A417-A424.

[36] N. Yabuuchi, K. Yamamoto, K. Yoshii, I. Nakai, T. Nishizawa, A. Omaru, T. Toyooka, S. Komaba, *J. Electrochem. Soc.* 2013, **160**, A39-A45.

[37] M. Gu, I. Belharouak, J. Zheng, H. Wu, J. Xiao, A. Genc, K. Amine, S. Thevuthasan, D. R. Baer, J.-G. Zhang, N. D. Browning, J. Liu, C. Wang, *ACS Nano* 2013, **7**, 760-767.

View Article Online
DOI: 10.1039/C6TA10577G

[38] F. Amalraj, M. Talianker, B. Markovsky, D. Sharon, L. Burlaka, G. Shafir, E. Zinigrad, O. Haik, D. Aurbach, J. Lampert, M. Schulz-Dobrick, A. Garsuch, *J. Electrochem. Soc.* 2013, **160**, A324-A337.

[39] P. K. Nayak, J. Grinblat, M. Levi, D. Aurbach, *Electrochimica Acta* 2014, **137**, 546–556.

[40] X. Yu, Y. Lyu, L. Gu, H. Wu, S.-M. Bak, Y. Zhou, K. Amine, S. N. Ehrlich, H. Li, K.-W. Nam, X.-Q. Yang, *Adv. Energy Mater.* 2014, **4**, 1300950.

[41] P. K. Nayak, J. Grinblat, M. Levi, O. Haik, E. Levi, D. Aurbach, *J. Solid State Electrochem*. 2015, **19,** 2781–2792.

[42] P. K. Nayak, J. Grinblat, M. Levi, O. Haik, E. Levi, Y.-K. Sun, N. Munichandraiah, D. Aurbach, *J. Mater. Chem. A* 2015, **3**, 14598–14608.

[43] P. K. Nayak, J. Grinblat, M. Levi, B. Markovsky, D. Aurbach, *J. Power Sources* 2016, **318**, 9-17.

[44] J. C. Knight, A. Manthiram, *J. Mater. Chem. A* 2015, **3**, 22199–22207.

[45] M. D. Levi, V. Dargel, Y. Shilina, I. Halalay, D. Aurbach, *Electrochim. Acta* 2014, **149**, 126-135.

View Article Online
DOI: 10.1039/C6TA10577G

TOC figure:

Lithium doping improves structural stability and increases average working potential of manganese oxide cathodes for Sodium-ion batteries.